Involvement of Smi1 in cell wall integrity and glucan synthase Bgs4 localization during fission yeast cytokinesis

Larissa V. G. Longo[a], Evelyn G. Goodyear[a], Sha Zhang[a], Elena Kudryashova[b], and Jian-Qiu Wu[a,c,*]
[a]Department of Molecular Genetics, [b]Department of Chemistry and Biochemistry, and [c]Department of Biological Chemistry and Pharmacology, The Ohio State University, Columbus, OH 43210

ABSTRACT **Cytokinesis is the final step of the cell-division cycle. In fungi, it relies on the coordination of constriction of an actomyosin contractile ring and construction of the septum at the division site. Glucan synthases synthesize glucans, which are the major components in fungal cell walls and division septa. It is known that Rho1 and Rho2 GTPases regulate glucan synthases Bgs1, Bgs4, and Ags1, and that Sbg1 and the F-BAR protein Cdc15 play roles in Bgs1 stability and delivery to the plasma membrane. Here we characterize Smi1, an intrinsically disordered protein that interacts with Bgs4 and regulates its trafficking and localization in fission yeast. Smi1 is important for septum integrity, and its absence causes severe lysis during cytokinesis. Smi1 localizes to secretory vesicles and moves together with Bgs4 toward the division site. The concentrations of the glucan synthases Bgs1 and Bgs4 and the glucanases Agn1 and Bgl2 decrease at the division site in the *smi1* mutant, but Smi1 seems to be more specific to Bgs4. Mistargeting of Smi1 to mitochondria mislocalizes Bgs4 but not Bgs1. Together, our data reveal a novel regulator of glucan synthases and glucanases, Smi1, which is more important for Bgs4 trafficking, stability, and localization during cytokinesis.**

Monitoring Editor
Rong Li
Johns Hopkins University and National University of Singapore

Received: Apr 28, 2021
Revised: Nov 29, 2021
Accepted: Dec 8, 2021

INTRODUCTION

Cytokinesis is the final step of the cell-division cycle, which partitions cellular contents from a mother cell into two daughter cells. Cytokinesis in fungi relies on successful coordination of assembly and constriction of an actomyosin contractile ring, plasma membrane deposition at the division site, and construction and remodeling of the division septum (Proctor *et al.*, 2012; Thiyagarajan *et al.*, 2015; Zhou *et al.*, 2015; Meitinger and Palani, 2016; Pollard, 2019). Several cellular pathways involved in the regulation of these processes have been discovered, but the molecular mechanisms behind septum synthesis remain poorly understood.

In the fission yeast *Schizosaccharomyces pombe* and most fungi, the septum is composed mainly of glucans and has three layers with a primary septum sandwiched by secondary septa. Daughter cells separate when the primary septum is digested by glucanases and the secondary septa become the cell wall of new cell ends (Alonso-Nunez *et al.*, 2005). Septum synthesis in *S. pombe* primarily depends on three glucan synthases: Bgs1, Bgs4, and Ags1. The primary septum is mainly composed of linear β-(1,3) glucan synthesized by Bgs1 (Cortes *et al.*, 2002). Bgs4 synthesizes branched β-(1,3) glucan for secondary septum formation and the proper completion of primary septa (Muñoz *et al.*, 2013). Ags1 is responsible for α-(1,3) glucan synthesis, which is found in the secondary septum and strengthens the primary septum (Cortes *et al.*, 2012). These three glucan synthases are all essential transmembrane proteins that are delivered to the plasma membrane at the division site via the secretory pathway (Liu *et al.*, 1999; Cortes *et al.*, 2002, 2005, 2012; Muñoz *et al.*, 2013).

Several regulators of the conserved glucan synthases have been identified in fungi, such as Rho GTPases (Drgonova *et al.*, 1996; Kondoh *et al.*, 1997; Beauvais *et al.*, 2001) and the α-COP protein, which is involved in their intracellular translocation from endoplasmic reticulum to Golgi (Lee *et al.*, 1999; Lee *et al.*, 2002). In *S. pombe*, β-glucan synthases Bgs1 and Bgs4 are activated by Rho1 GTPase (Arellano *et al.*, 1996), and Rho1 and Rho2 GTPases regulate the α-glucan synthase Ags1 through the protein kinase C Pck2

This article was published online ahead of print in MBoC in Press (http://www.molbiolcell.org/cgi/doi/10.1091/mbc.E21-04-0214) on December 15, 2021.

*Address correspondence to: Jian-Qiu Wu (wu.620@osu.edu).

Abbreviations used: GBP, GFP-binding protein; IDP, intrinsically disordered protein; PB, phloxin B; SPB, spindle pole body; TIRF, total internal reflection fluorescence; WT, wild type.

(Katayama *et al.*, 1999; Calonge *et al.*, 2000). We and others have previously identified Sbg1 as a novel regulator for the localization and stability of Bgs1 and found that Sbg1 is important for actomyosin ring constriction and septum synthesis (Davidson *et al.*, 2016; Sethi *et al.*, 2016). Bgs1 transport also depends on the F-BAR protein Cdc15 and clathrin light chain Clc1 (de Leon *et al.*, 2013; Arasada and Pollard, 2014). Cdc15 helps deliver Bgs1 from the Golgi to the plasma membrane, where the Bgs1–Cdc15 interaction is important for contractile ring stability (Arasada and Pollard, 2014), while β-glucan synthase activity is diminished and Bgs1 localization is compromised without Clc1 (de Leon *et al.*, 2013). Furthermore, the F-BAR protein Rga7 is critical for the delivery of Bgs4 to the cleavage site (Arasada and Pollard, 2015), and both *rga7*Δ and coiled-coil protein *rng10*Δ mutants reduce Bgs1, Bgs4, and Ags1 levels at the division site (Liu *et al.*, 2016). However, much remains unknown about the coordination of these glucan synthases and the mechanisms of their delivery to and localization at the division site.

Smi1, also known as Knr4, is an intrinsically disordered protein (IDP) conserved in many fungi (Martin-Yken *et al.*, 2016). In *Saccharomyces cerevisiae*, Smi1 acts as a hub that physically interacts with the key components of two pathways: Slt2 MAP kinase in the cell wall integrity pathway and the calcineurin phosphatase in the calcium–calcineurin pathway (Dagkessamanskaia *et al.*, 2010a,b; Martin-Yken *et al.*, 2016). The roles of Smi1 as a hub are also supported by its numerous interaction partners, including many synthetic lethal interactions (Goehring *et al.*, 2003; Costanzo *et al.*, 2010). Smi1 also regulates transcription of genes involved in cell cycle, cell wall synthesis, morphogenesis, and transcriptional responses to heat and cell wall stress in different fungi (Martin-Yken *et al.*, 2002; Lagorce *et al.*, 2003; Penacho *et al.*, 2012). In the *smi1* mutant, the SBF transcription factor is constitutively hyperactivated instead of peaking at the G1/S transition (Kim *et al.*, 2010), and at least two cell cycle checkpoints are impaired: the morphogenesis checkpoint, which coordinates cell division with bud growth (Harrison *et al.*, 2001; Mizunuma *et al.*, 2001; Miyakawa and Mizunuma, 2007) and the mechanism controlling the daughter cell size (Dagkessamanskaia *et al.*, 2010a,b). Smi1 homologues in other fungi exhibit similar functions and localization at polarized growth sites (Martin-Yken *et al.*, 2003). However, it has not been reported that Smi1 directly regulates glucan synthases or glucanases in budding yeast and other fungi.

In this study, we investigated the role of the essential protein Smi1 in the regulation of septum formation and cell separation in fission yeast cytokinesis. We found that Smi1 and Bgs4 physically interact, colocalize in secretory vesicles, and travel together toward the division site. Localizations of glucan synthases, especially Bgs4, depend on Smi1. Collectively, we conclude that Smi1 is important for Bgs4 trafficking and localization to regulate late stages of cytokinesis in fission yeast.

RESULTS

Identification of Smi1 as a β-glucan synthase Bgs4 binding partner

Identification of binding partners of glucan synthases, which are essential for cell wall and septum formation, is important for understanding the synthases' functions. Recently, our lab and others characterized transmembrane protein Sbg1 as a regulator of the β-glucan synthase Bgs1 (Davidson *et al.*, 2016; Sethi *et al.*, 2016), which led us to search for Bgs4 binding partners. Purification of GFP-Bgs4 from an *S. pombe* extract using GFP-Trap (Rothbauer *et al.*, 2008) followed by mass spectrometry identified Smi1 (SPBC30D10.17c) as a Bgs4-interacting protein (Supplemental Figure S1). Smi1 was more abundant in pull downs of cells expressing GFP-Bgs4 than in those from GFP-Bgs1 (Supplemental Figure S1A). Additionally, Smi1 coverage was higher from cells expressing GFP-Bgs4 than GFP-Bgs1 (Supplemental Figure S1B). Predictive modeling of Smi1 suggested that the N- (aa 1–130) and C- (aa 340–504) terminal regions of Smi1 are highly disordered, while its central portion (aa 131–339), which contains the Smi1/Knr4 domain (aa 153–301), is structured (Figure 1, A and B). The same pattern of disordered N- and C-termini and a structured central region was observed in the Smi1 homologue Knr4 in *S. cerevisiae* (Martin-Yken *et al.*, 2016).

Smi1 is important for septum integrity

Smi1 has been previously described as an essential gene in *S. pombe* genome-wide studies (Kim *et al.*, 2010; Hayles *et al.*, 2013). It was reported that Smi1 is involved in the entry and maintenance of the quiescent state (Sajiki *et al.*, 2009). To investigate the roles of Smi1 in cycling cells, we generated a *smi1-1* temperature-sensitive mutant (Figure 1B) by marker reconstitution mutagenesis (Tang *et al.*, 2011). *smi1-1* had three mutations, one in the disordered C-terminus and two in the central ordered region (Figure 1B). The major phenotype of *smi1-1* was massive cell lysis, with ~76% of cells lysed at the restrictive temperature (Figure 1, C and D). Time-lapse microscopy revealed that lysis occurred during cell separation, and either one or both daughter cells of *smi1-1* lysed (Figure 1E; Supplemental Movie S1). *smi1-1* cells also showed a significantly higher (38.5%) septation index than wild-type (WT) cells (11.5%) at 36°C (Figure 1F). The cell lysis and septation defects were confirmed by depleting Smi1 using *P81nmt1-smi1* cells in medium containing thiamine (Supplemental Figure S2, A–D).

The *smi1-1* lysis phenotype suggested a possible role of Smi1 in cell wall integrity during septation. Indeed, *smi1-1* cells were sensitive to cell wall stresses including treatments with Calcofluor white and SDS, indicating a cell wall weakness (Figure 2A). This phenotype was rescued by sorbitol, which decreased the osmotic stress on the weakened cell wall (Figure 2A). Genetic evidence also supported that Smi1 works with glucan synthases for septum synthesis and cell wall integrity. *smi1-1* was synthetic lethal with mutations in β-glucan synthases Bgs1 (*bgs1-191* and *bgs1-D277N* [Liu *et al.*, 1999; Dundon and Pollard, 2020]) and Bgs4 (*cwg1-1* and *cwg1-2* [Ribas *et al.*, 1991; Muñoz *et al.*, 2013]) at 30°C (Figure 2B and Table 1) and showed moderate genetic interaction with the α-glucan synthase Ags1 mutant *mok1-664* (Katayama *et al.*, 1999) (Table 1). In addition, *smi1-1* had strong genetic interactions with mutations in the cell integrity pathway (protein kinase Cs *pck1*Δ and *pck2-Δ1* [Toda *et al.*, 1993; Viana *et al.*, 2013] and arrestin *art1*Δ [Davidson *et al.*, 2015]), in glucan synthase regulators *rga7*Δ and *rng10*Δ (Nakano *et al.*, 2001; Kim *et al.*, 2010; Liu *et al.*, 2016, 2019), and in the septum initiation network (*mob1-M17* [Salimova *et al.*, 2000]) (Figure 2B and Table 1).

We confirmed the defects in septa using electron microscopy. In cells with closed septa, the primary septum was uneven (Figure 3, red arrows) and thinner in *smi1-1* cells than in WT (Figure 3A). The defects in the septum and cell wall adjacent to the division site were more obvious in separating *smi1-1* cells (Figure 3B). Unilateral separation with a thinned adjacent cell wall was frequently observed in *smi1-1* cells (Figure 3B, black arrows). Similar defects were seen when Smi1 was depleted (Supplemental Figure S2D), indicating that the septal defects were due to the lack of Smi1 function. Moreover, *smi1-1* cells had lower Calcofluor intensity at the division site, which stains the primary septum (Figure 3C), confirming an impaired primary septum.

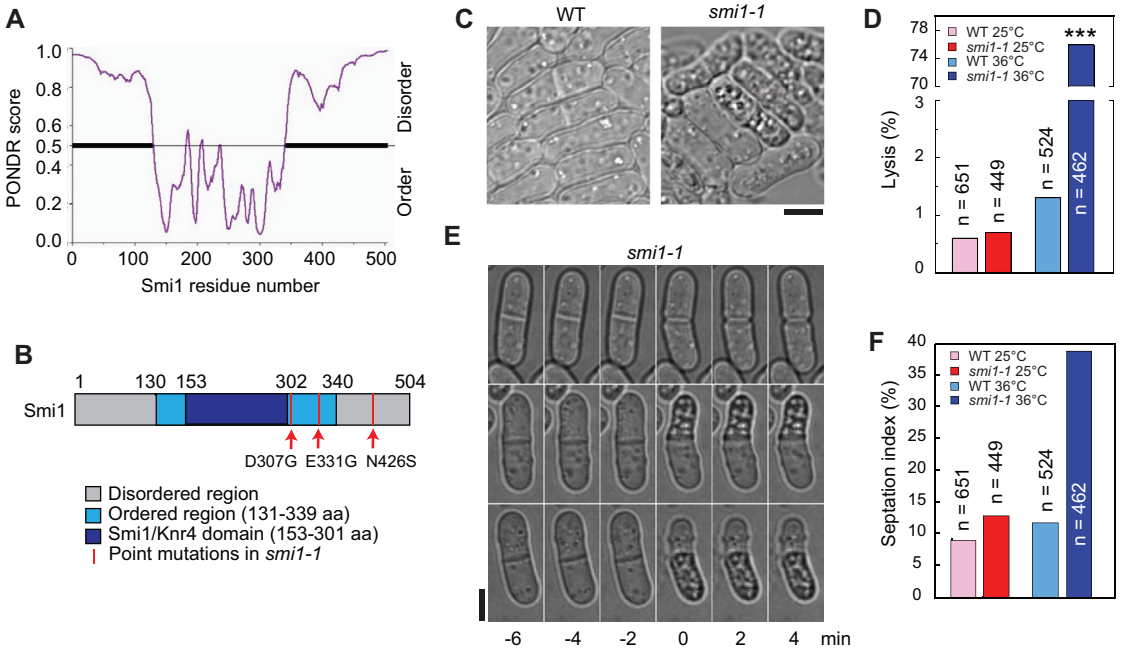

FIGURE 1: The intrinsically disordered protein Smi1 is important for cell integrity during cell separation. (A) Computational evaluation of intrinsic disorder propensity of Smi1 using PONDR-VSL1 score (http://www.pondr.com/). Values between 0 and 1 are scored considering amino acid frequencies, sequence complexity, ratio of net charge/hydrophobicity, and mean flexibility. Scores ≥0.5 indicate disorder. (B) Schematic of Smi1 domain organization, highlighting the three point mutations in *smi1-1*: D307G, E331G, and N426S. (C) DIC images of *smi1-1* cells grown at 36°C for 4 h. (D) Quantification of cell lysis in WT and *smi1-1* cells grown at 25°C or shifted to 36°C for 4 h. (E) Time-lapse images of cell-lysis scenarios during separation of *smi1-1* cells at 36°C. None (top), one (middle), or both (bottom) daughter cells lysed are shown. Scale bars, 5 µm. See also Supplemental Movie S1. (F) Quantification of septation index in WT and *smi1-1* cells grown at 25°C or shifted to 36°C for 4 h. ***$p < 0.0001$ compared with WT in *t* test.

The glucan synthases are transmembrane proteins delivered to the plasma membrane via the secretory pathway (Liu *et al.*, 1999; Cortes *et al.*, 2002, 2005, 2012; Muñoz *et al.*, 2013). To investigate the potential role of Smi1 in exocytosis, *smi1-1* was crossed with different mutants in the exocytic pathway (Table 1), but only moderate genetic interactions with Munc13/UNC-13 mutant *ync13-4* (Zhu *et al.*, 2018) and the myosin-V mutant *myo52*Δ (Motegi *et al.*, 2001; Win *et al.*, 2001) were detected, suggesting that Smi1 is not a general player in the exocytic pathways. Interestingly, *smi1-1* showed only mild genetic interactions with mutations in contractile ring

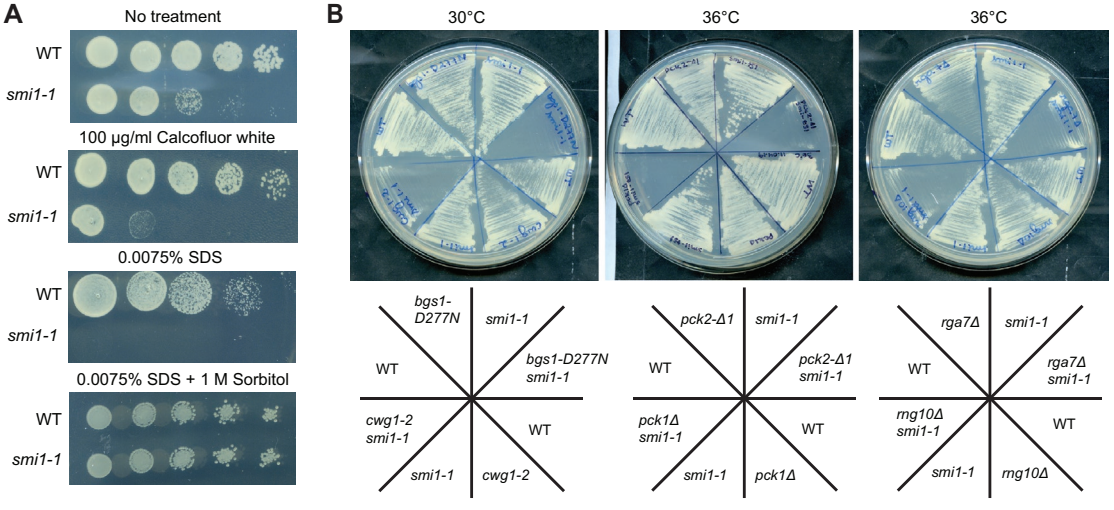

FIGURE 2: Smi1 plays a role in cell wall integrity. (A) Sensitivity of *smi1-1* cells to Calcofluor white and SDS. Cells were grown in YE5S medium (25°C), spotted in serial (five-fold) dilutions onto YE5S plates and YE5S plates containing the indicated treatments, and then incubated at 36°C for 48 h. (B) Synthetic genetic interactions between *smi1-1* and mutations in genes involved in cell wall integrity. The cells were grown on YE5S plates at 30 or 36°C for 48 h.

Mutations	25°C	30°C	36°C
smi1-1	+++	++	+
Contractile ring			
pxl1Δ	+++	+++	+++
pxl1Δ smi1-1	+++	++	+
myo2-E1	+++	+++	++
myo2-E1 smi1-1	+++	+	–
cdc15-140	+++	+	–
cdc15-140 smi1-1	+++	+	–
mid1-6	+++	+++	++
mid1-6 smi1-1	+++	++	+
Glucan synthases and glucanases			
bgs1-191	+++	++	–
bgs1-191 smi1-1	++	–	–
bgs1-D277N	++	++	+
bgs1-D277N smi1-1	+	–	–
cwg1-1	+++	+++	++
cwg1-1 smi1-1	+++	++	–
cwg1-2	+++	++	++
cwg1-2 smi1-1	+	–	–
mok1-664	+++	++	–
mok1-664 smi1-1	+++	+	–
chs2-Δ1	+++	+++	+++
chs2-Δ1 smi1-1	+++	++	+
agn1Δ	+++	+++	++
agn1Δ smi1-1	+++	++	+
eng1Δ	+++	+++	+++
eng1Δ smi1-1	+++	++	+
exg1Δ	+++	+++	++
exg1Δ smi1-1	+++	++	+
Cell integrity pathway (CIP)			
rho1-596	++	+	–
rho1-596 smi1-1	++	+	–
rho2Δ	+++	++	++
rho2Δ smi1-1	+++	++	+
rga7Δ	++	+	+
rga7Δ smi1-1	++	+	–
rng10Δ	++	++	+
rng10Δ smi1-1	++	+	–
art1Δ	++	++	++
art1Δ smi1-1	++	+	–
pck1Δ	+++	+++	+++
pck1Δ smi1-1	++	+	–
pck2-Δ1	+++	++	++
pck2-Δ1 smi1-1	+++	+	–
spn1-Δ2	+++	++	++
spn1-Δ2 smi1-1	+++	++	+
myp2-Δ2	+++	+++	+++
myp2-Δ2 smi1-1	+++	++	+
rgf3-s44	+	+	+
rgf3-s44 smi1-1	+	+	–
Septation initiation network (SIN)			
mob1-M17	+++	+++	++
mob1-M17 smi1-1	++	–	–
sid2-250	+	–	–
sid2-250 smi1-1	+	–	–
cdc7-24	++	–	–
cdc7-24 smi1-1	++	–	–
Exocytosis			
exo70Δ	+++	+++	++
exo70Δ smi1-1	+++	++	+
sec8-1	+++	+++	–
sec8-1 smi1-1	+++	++	–
trs120-M1	++	–	–
trs120-M1 smi1-1	++	–	–
trs120-1	+++	+++	–
trs120-1 smi1-1	+++	++	–
ync13-19	+	–	–
ync13-19 smi1-1	+	–	–
ync13-4	+++	++	+
ync13-4 smi1-1	++	+	–
myo52Δ	++	++	+
myo52Δ smi1-1	++	++	–
mso1Δ	+++	+++	–
mso1Δ smi1-1	+++	++	–
sec1-M2	+++	+++	++
sec1-M2 smi1-1	+++	++	+
Endocytosis			
pan1ΔACV	+++	+++	++
pan1ΔACV smi1-1	+++	++	+
fim1-Δ1	+++	++	+
fim1-Δ1 smi1-1	+++	++	+
end4Δ[a]	–	–	–
end4Δ smi1-1	++	++	++

Strong genetic interactions are highlighted in gray. +++, growth and morphology similar to WT; ++, some cell lysis, pink color on YE5S + PB plates; +, massive cell lysis, red color on YE5S + PB plates; –, inviable, unable to grow on YE5S + PB plates.

[a]Strain was woken up in YE5S + sorbitol plates, because it does not grow on YE5S plates.

TABLE 1: Genetic interactions between mutations in *smi1* and genes involved in cytokinesis.

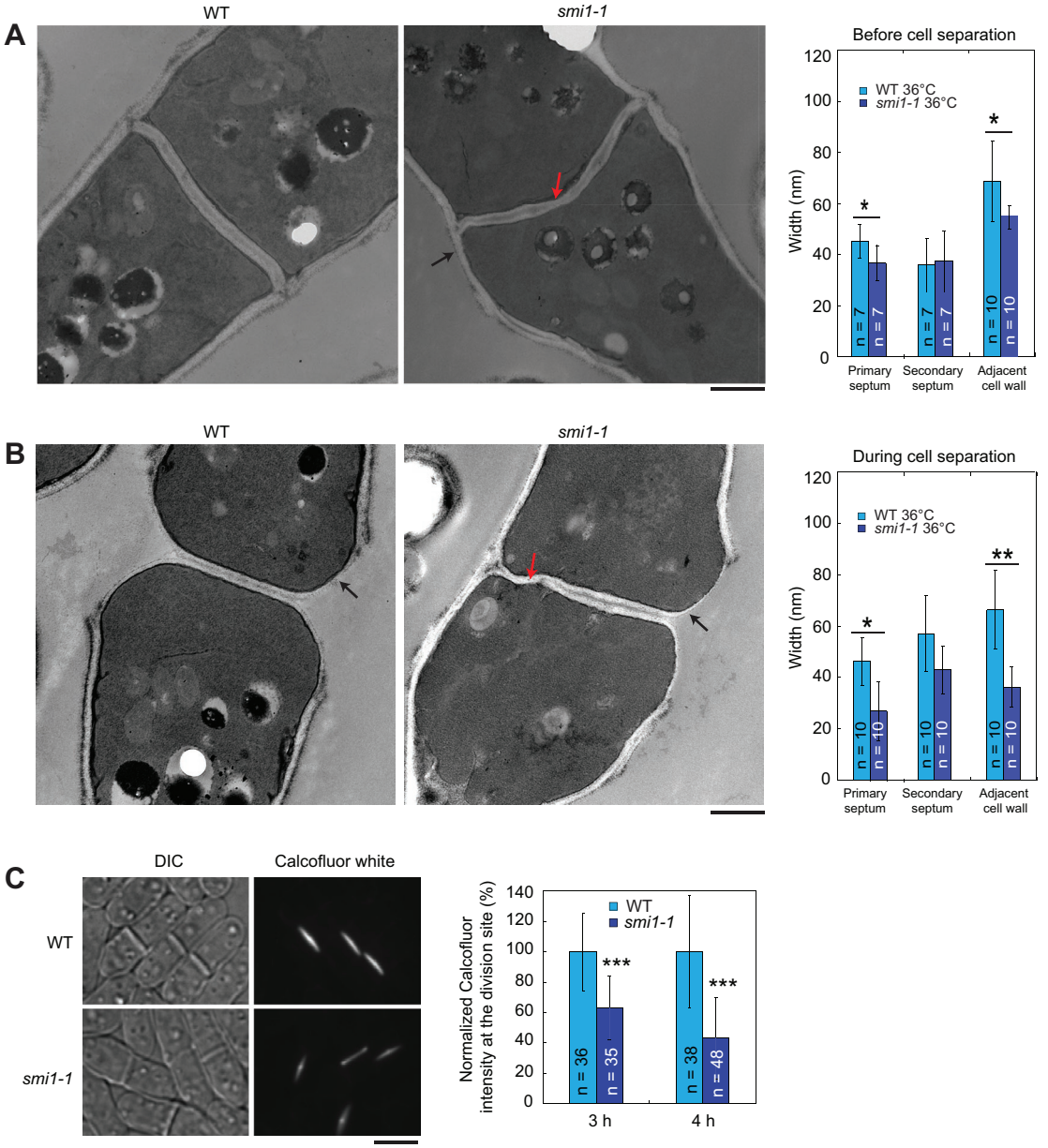

FIGURE 3: Smi1 plays a role in septum and cell wall formation during septation. (A, B) Electron microscopy micrographs (left and middle) and quantifications of septum width (right) of septating WT and *smi1-1* cells grown at 36°C for 4 h before (A) or during (B) daughter-cell separation. The red arrow marks defects in the primary septum, and the black arrows indicate the thinner adjacent cell wall (within 0.5 µm from the septum). Asymmetric separation in *smi1-1* is also shown. Scale bars, 500 nm. (C) Micrographs and quantifications of defective primary septa in *smi1-1* cells grown at 36°C for 3–4 h, as revealed by Calcofluor white staining. Scale bar, 5 µm. *$p < 0.01$, **$p < 0.001$, and ***$p < 0.0001$ compared with WT.

components (Balasubramanian *et al.*, 1998), suggesting that the ring machinery is not affected by the *smi1* mutation (Table 1). Indeed, time-lapse microscopy revealed that the timing of ring formation, maturation, constriction, and disassembly was similar in *smi1-1* and WT cells (Supplemental Figure S3). Collectively, the lysis phenotype, high septation index, genetic interactions, and electron microscopy data indicate that Smi1 is important for septum formation and/or cell septation.

Smi1 localizes to the division site and secretory vesicles

To better understand Smi1 function during cytokinesis, we tagged Smi1 at its C-terminus under its native promoter with tandem dimer Tomato (tdTomato) and monomeric enhanced GFP (mEGFP). Smi1 localized to cytoplasmic puncta and the division site (Figure 4A, arrows), forming a discrete ring in 87% ($n = 300$) of dividing cells in time-lapse movies (Figure 4B). With the spindle pole body (SPB) protein Sad1 as a cell cycle marker, we observed that Smi1 started to concentrate at the division site 18 ± 4 min ($n = 15$ cells) after SPB separation (Figure 4C, yellow arrow). To determine the identity of the Smi1 puncta, we compared Smi1 localization to known vesicle proteins at different stages of secretion (Figure 4, D and E). Smi1 puncta colocalized well with *trans*-Golgi marker Sec72 (Vjestica *et al.*, 2008); ~80% Smi1 puncta contained Sec72 (Figure 4E) while <40% Smi1 puncta colocalized with early Golgi proteins Anp1 and

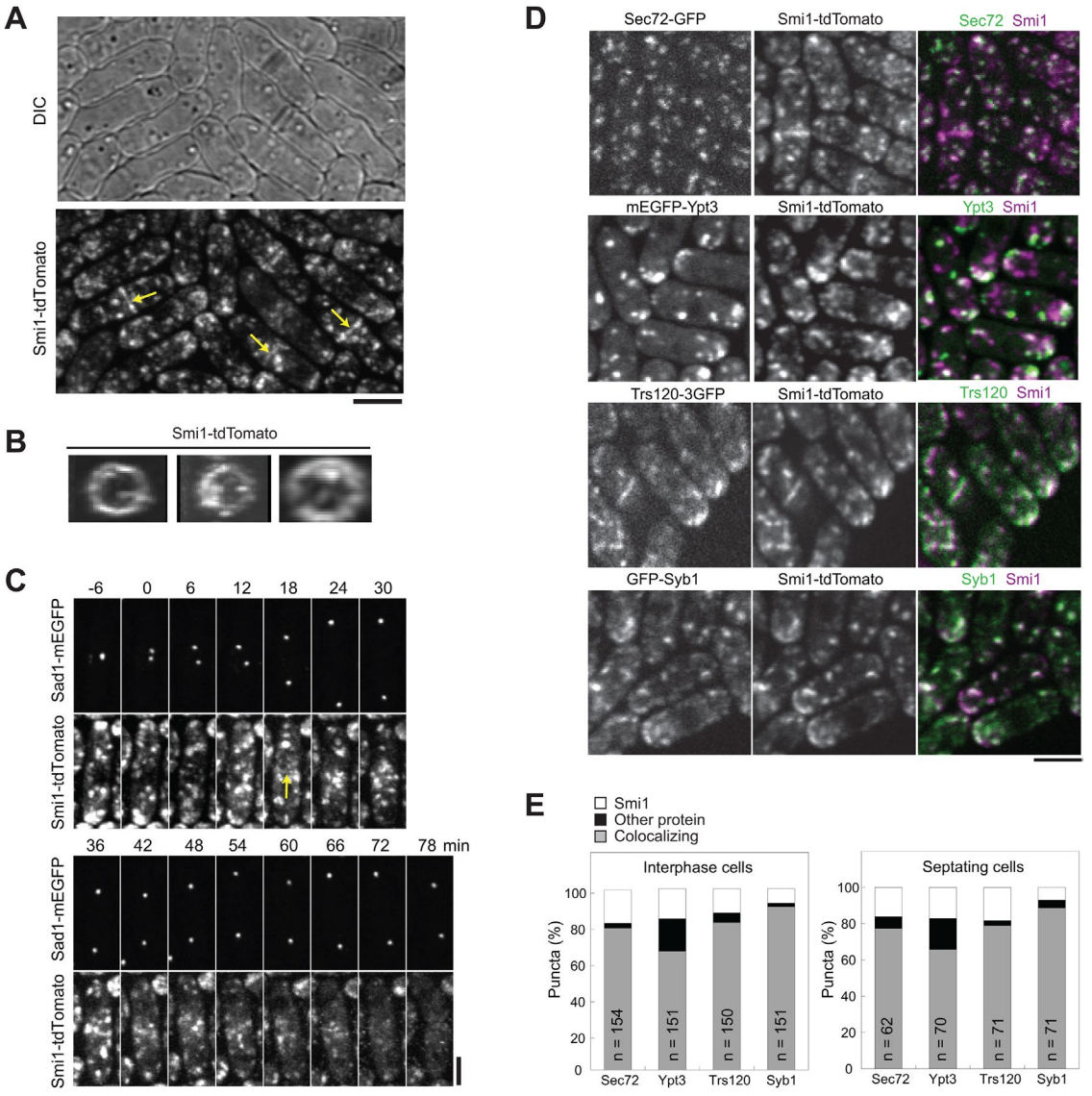

FIGURE 4: Localization of Smi1 to secretory vesicles and the division site. (A) Smi1 localizes to cytoplasmic puncta and the division site (arrows). (B) Three-dimensional projection of Smi1-tdTomato forming a ring structure at the division site in three different cells. (C) Time course of Smi1 localization with SPB protein Sad1 (its separation defined as time 0) as a cell cycle marker. (D, E) Micrographs (D) and quantifications (E) showing the colocalization of Smi1 with Sec72, Ypt3, Trs120, and Syb1 in vesicles in interphase and septating cells. *N* = number of vesicles in ~10 cells for each protein. Scale bars, 5 μm.

Sec24 (Supplemental Figure S4). Smi1 also colocalized well with the Rab11 family GTPase Ypt3, the TRAPP II complex subunit Trs120, and the v-SNARE Syb1 (Figure 4, D and E). The localization is consistent with Smi1's roles in septum formation and/or cell septation.

Smi1 colocalizes with glucan synthases

To better understand the role of Smi1 in septum synthesis, we investigated the colocalization of Smi1 with glucan synthases (Figure 5). Whether the cells were in interphase or septating, Smi1 colocalized well in cytoplasmic puncta with glucan synthases Bgs4 (90–93%), Ags1 (82–87%), Bgs1 (65–76%), and the Bgs1 partner Sbg1 (76–79%), although Smi1 was less concentrated on the plasma membrane (Figure 5, A and B). A parallel analysis was performed to compare the colocalization between the glucan synthases Bgs1, Bgs4, and Ags1 (Supplemental Figure S5). No colocalization higher than 85% was seen in cytoplasmic puncta, suggesting that the high rate of colocalization between Bgs4 and Smi1 is specific. Thus, we analyzed GFP-Bgs4 and Smi1-tdTomato trafficking by total internal reflection fluorescence (TIRF) microscopy. We found that Smi1 and Bgs4 traveled in vesicles and arrived at the division site together (Figure 5C, *n* = 12; Supplemental Movie S2). These data support a role for Smi1 in glucan synthase delivery to the division site, especially for Bgs4.

To further investigate the relationship between Smi1 and glucan synthases, we mislocalized Smi1 using the mitochondrial outer membrane protein Tom20 tagged with GFP-binding protein (GBP; Figure 6). Smi1-mEGFP mislocalized Bgs4 and Ags1 to mitochondria, where they colocalized in mitochondrial strands or clumps throughout the cell (Figure 6, A and B, yellow arrows). In contrast, Bgs1 and Sbg1 were not mislocalized by Smi1-mEGFP (Figure 6, C and D). The reverse experiments showed that only the mistargeted GFP-Bgs4, but not Ags1, Bgs1, or Sbg1, could mislocalize Smi1 to the mitochondria

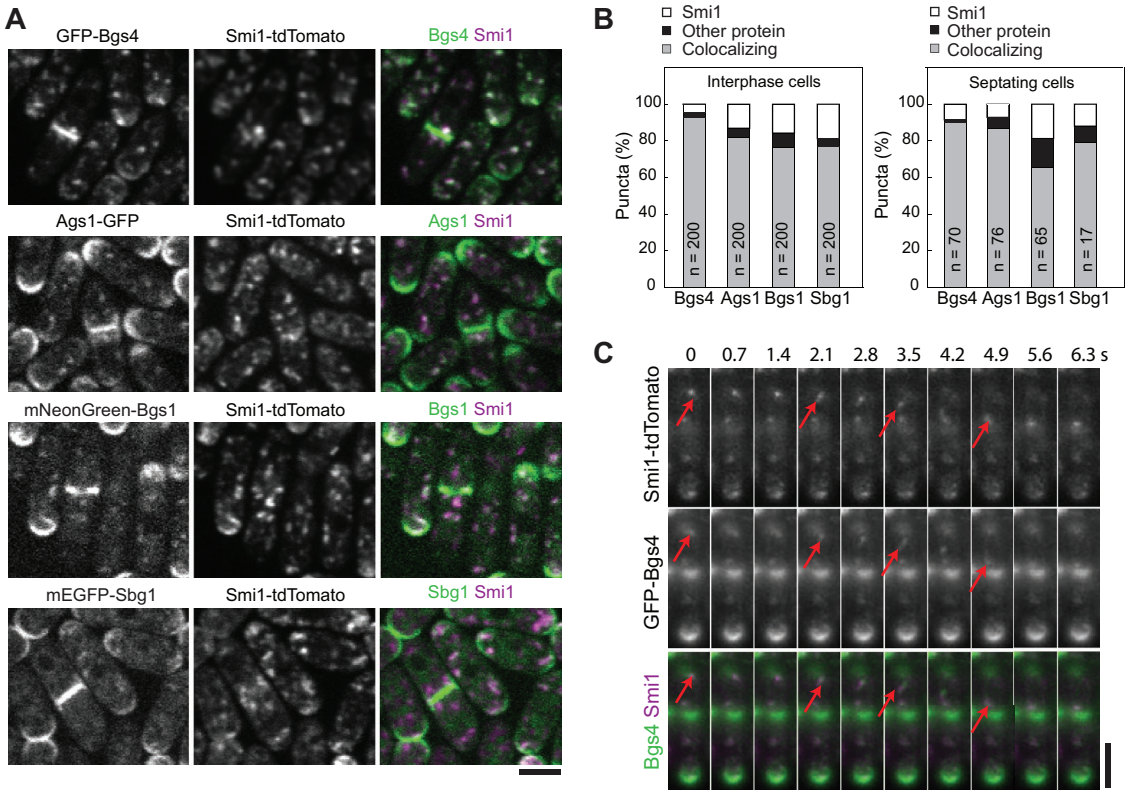

FIGURE 5: Smi1 mostly colocalizes with Bgs4, Ags1, Bgs1, and Sbg1 and travels together with Bgs4 in vesicles. Micrographs (A) and quantifications (B) showing colocalization of Smi1 with Bgs4, Ags1, Bgs1, and Sbg1 in vesicles in interphase and septating cells. (C) TIRF micrographs showing that Smi1 and Bgs4 move together in vesicles (an example marked by a red arrow) to the division site. Scale bars, 5 μm. See also Supplemental Movie S2.

(Supplemental Figure S6). This could be due to a weaker interaction between Ags1 and Smi1 in comparison to that between Bgs4 and Smi1 or different configurations of proteins on the outer membrane of mitochondria. Consistently, we found that Smi1 coimmunoprecipitated with Bgs4 (Figure 6E). We confirmed that the mislocalization was not caused by signal bleed-through between channels (Supplemental Figure S7). Together, these results suggested that Smi1 interacts with Bgs4, which is important for Bgs4 localization.

Smi1 helps to deliver glucan synthases and glucanases to the division site

To understand the importance of Smi1 for localization of glucan synthases, we measured their fluorescence intensities in the *smi1-1* mutant (Figure 7). Bgs4 had lower global intensity in *smi1-1* cells, while that of Ypt3, Ags1, Bgs1, and Sbg1 remained the same as in WT cells (Figure 7, A and B). This Bgs4 result was confirmed by Western blot showing that the *smi1-1* strain had a lower GFP-Bgs4 level compared with WT control (Figure 7D). Together, these results suggest that Smi1 plays a role in Bgs4 stability or expression level.

The local intensity of Bgs1, Bgs4, and Sbg1, but not Ags1, at the division site was significantly lower in *smi1-1* than WT cells in all cytokinesis stages. The Bgs4 level at the division site decreased the most, >80%, which is higher than the decrease in global intensity (Figure 7, A–D). The Bgs4 level at the cell tip of interphase cells was also dramatically decreased, and the cytoplasmic puncta looked more diffuse in *smi1-1* (Figure 7A). Line scan analyses of cytoplasmic puncta showed that Bgs4 intensity indeed decreased in *smi1-1* cells in comparison to WT (Figure 7E). This decrease in local intensity was specific to the glucan synthases studied, as the levels of the Rab11 GTPase Ypt3, a general regulator of vesicle trafficking at the plasma membrane (Cheng *et al.*, 2002), and contractile ring component Myo2 at the division site were not significantly altered in *smi1-1* cells (Figure 7, A and C, Supplemental Figure S3A, and unpublished data). In addition, localization and intensity of Ypt3 and Syb1 in cytoplasmic puncta were similar in *P81nmt1-smi1* and WT cells grown under repression condition (Supplemental Figure S8).

Previously, our group showed that Sbg1 is involved in Bgs1 localization and trafficking to the division site (Davidson *et al.*, 2016). To compare the importance of Smi1 and Sbg1 in the localization of glucan synthases, we measured the local intensity of Bgs1, Bgs4, and Ags1 at the division site in the temperature-sensitive mutant *sbg1-3* (Sethi *et al.*, 2016). Bgs1, but not Bgs4 or Ags1, intensity at the division site was reduced during the late stage of septation (Supplemental Figure S9). Together, these results confirmed that Sbg1 is specific to Bgs1, while Smi1 regulates the levels of both Bgs4 and Bgs1 at the division site, with a more important role for Bgs4 (Figure 7, A–C).

To investigate whether cell lysis in the *smi1-1* mutant is due to improper digestion of the septum, we also measured the levels of glucanases at the division site. The endo-(1,3)-β-glucanase Eng1 and the (1,3)-α-glucanase Agn1 are the two most studied glucanases involved in septum degradation during cell separation (Martin-Cuadrado *et al.*, 2003; Dekker *et al.*, 2004). By contrast, glucanases Bgl2 and Exg1 are less studied (Duenas-Santero *et al.*, 2010). We analyzed the fluorescence intensity of Eng1, Agn1, Bgl2, and Exg1 at the division site in WT and *smi1-1* cells (Figure 8). Agn1 and Bgl2 intensities were significantly lower in both early and late stages of septation (Figure 8, A–C), while Eng1 intensity was not

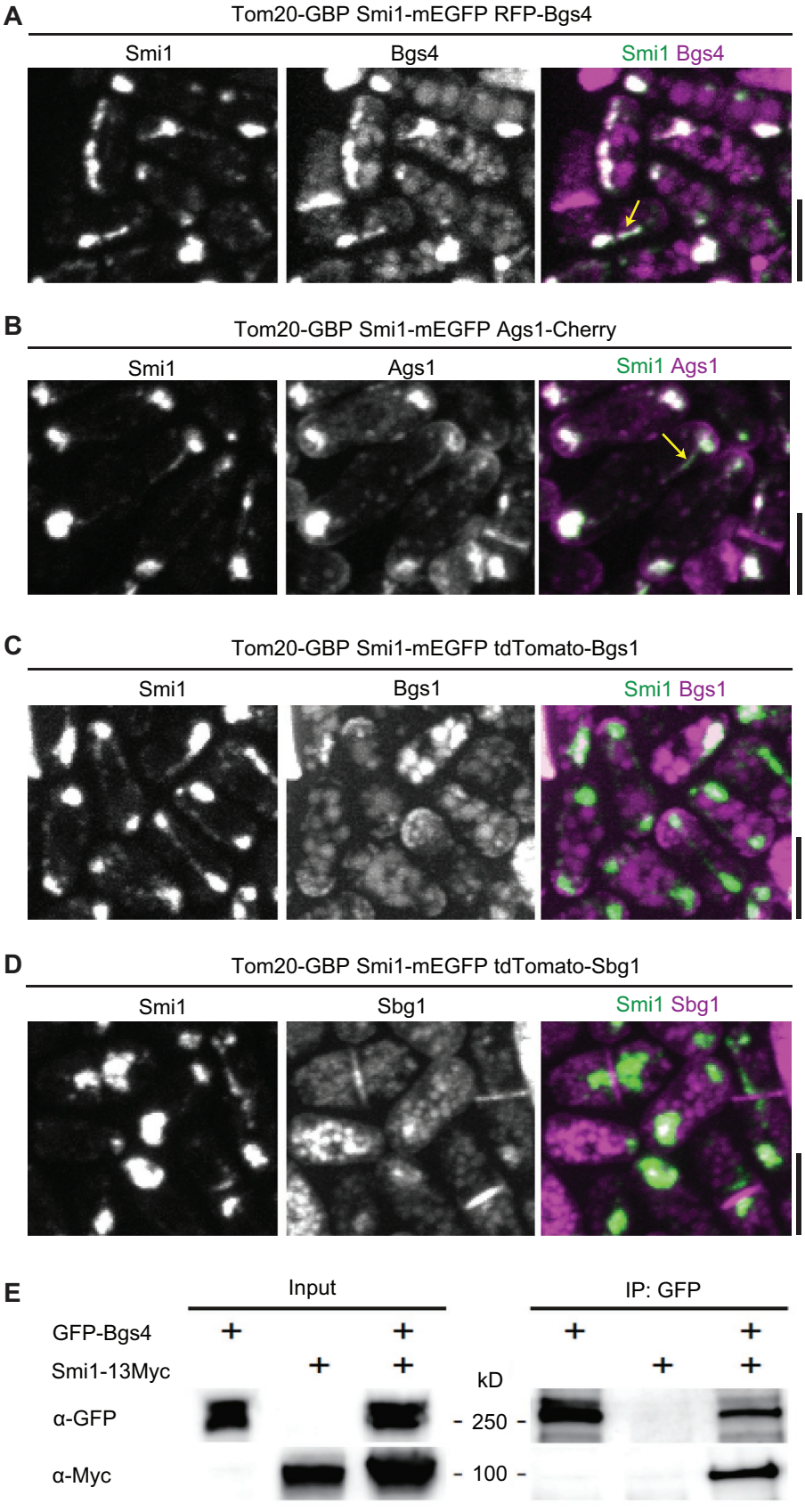

FIGURE 6: Mislocalized Smi1 can ectopically target Bgs4 and Ags1 to mitochondria. Micrographs of cells coexpressing Tom20-GBP, Smi1-mEGFP, and either RFP-Bgs4 (A), Ags1-Cherry (B), tdTomato-Bgs1 (C), or tdTomato-Sbg1 (D). Yellow arrows mark examples of colocalization on mitochondrial structures. Scale bars, 5 μm. (E) Smi1 coimmunoprecipitates with Bgs4. Solubilized proteins from the membrane fraction of the indicated strains were immunoprecipitated (IP) with anti-GFP antibodies. Proteins before (input) and after immunoprecipitation were transferred to the same membrane and blotted with monoclonal anti-GFP or anti-Myc antibody.

significantly reduced. Interestingly, the intensity of Exg1 increased in *smi1-1*, especially during early septation. However, the increased level of Exg1 was not the cause for cell lysis in *smi1-1* cells because the double mutant *smi1-1 exg1*Δ had a similar percentage of cell lysis as the *smi1-1* single mutant at the restrictive temperature (Supplemental Figure S10). Together, these results suggest that Smi1 has functions in maintaining the proper levels of both glucan synthases and glucanases at the division site.

DISCUSSION

In this study, we characterized Smi1, an intrinsically disordered protein that interacts with Bgs4 and regulates its trafficking and localization in fission yeast. Smi1 plays an essential role in maintaining septum integrity during the late stages of cytokinesis by regulating levels of glucan synthases (especially Bgs4) and glucanases at the division site to ensure proper cell division.

Roles of Smi1 in regulating septum integrity during cytokinesis

Except for its reported involvement in the entry and maintenance of quiescence (Sajiki *et al.*, 2009), the roles of Smi1 in fission yeast have not been studied. Our results provide several lines of evidence to suggest that Smi1 is important for septum integrity during cytokinesis. We showed that *smi1-1* cells had defective septa (Figure 3), which lead to massive cell lysis at restrictive temperature (Figure 1 and Supplemental Movie S1). Additionally, *smi1-1* was sensitive to cell wall stresses (Figure 2A) and was synthetic lethal with mutations in β-glucan synthases and the cell integrity pathway (Figure 2B and Table 1). Smi1 colocalized well with glucan synthases, especially Bgs4 (Figure 5 and Supplemental Movie S2), and Smi1 and Bgs4 physically interacted (Figure 6 and Supplemental Figure S6). Finally, the local intensities of the glucan synthases Bgs1 and Bgs4 and the glucanases Agn1, Bgl2, and Exg1 were significantly altered at the division site in *smi1-1* (Figures 7 and 8). Taken together, our data indicate that Smi1 plays important roles in septum integrity during the late stages of cytokinesis by regulating the proper delivery and localization of glucan synthases and glucanases to the division site.

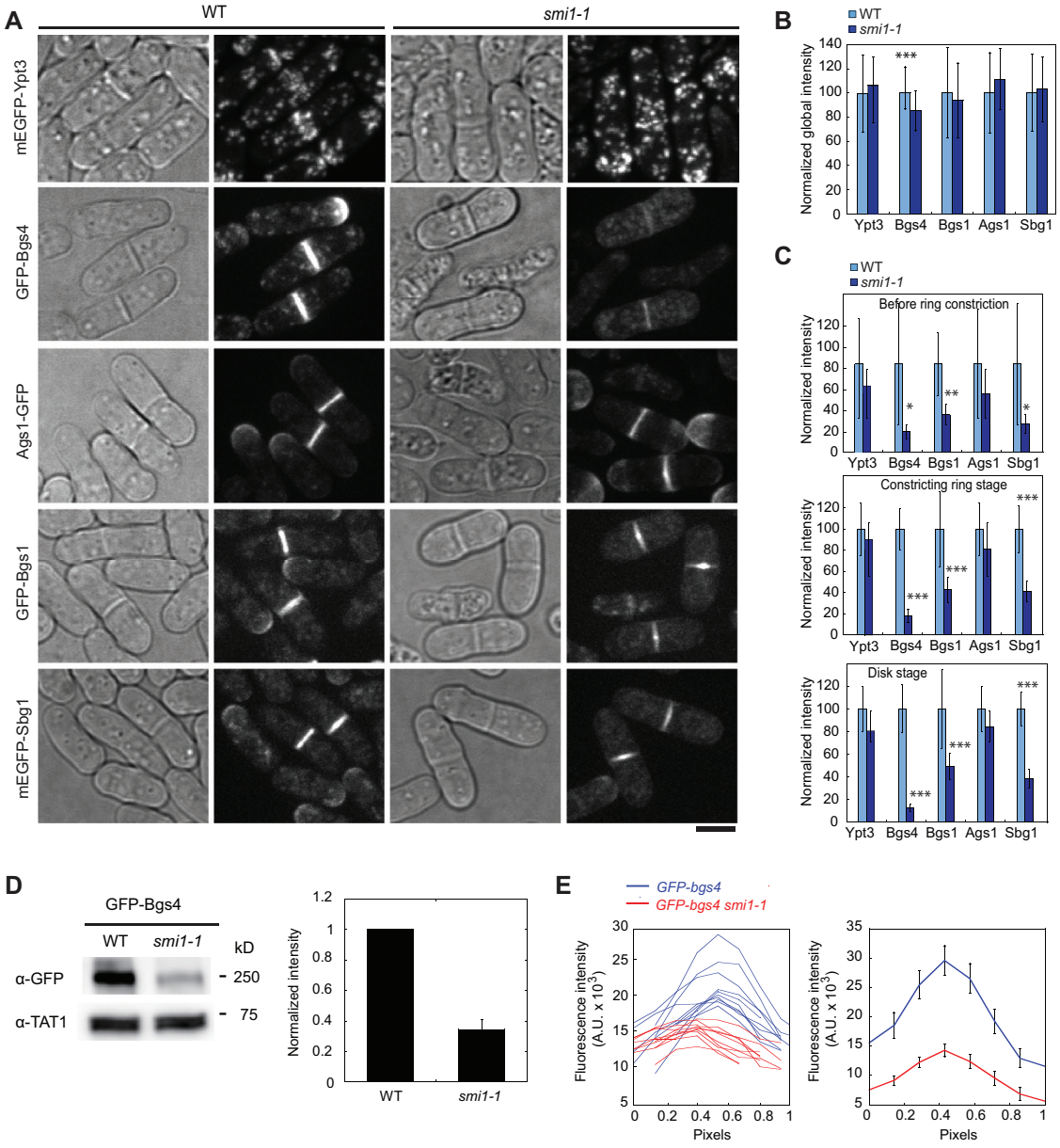

FIGURE 7: Localization of Ypt3, Bgs4, Ags1, Bgs1, and Sbg1 in WT and *smi1-1* cells. (A–C) DIC and maximum-intensity projections of fluorescence images (A), global fluorescence intensity (B, $n = 70$ cells each), and local intensity at the division site (C, $n = 15$ cells each) of Ypt3, Bgs4, Ags1, Bgs1, and Sbg1 in WT and *smi1-1* cells grown for 2 h at 36°C. Scale bar, 5 μm. For local fluorescence intensity, cells are grouped into three stages: before ring constriction (cells with compact ring before constriction), constricting ring (cells during ring constriction), and disk (cells with protein spreads to the whole division plane after ring constriction). *$p < 0.01$, **$p < 0.001$, and ***$p < 0.0001$ compared with the WT. (D) Western blot image (left) and quantification (right) of two independent experiments showing GFP-Bgs4 from whole cell lysates of *GFP-bgs4* and *smi1-1 GFP-bgs4* cells grown at 36°C for 2 h. α-TAT1 is a loading control. (E) Line scans of individual cell (left) and average (right; $n = 10$ cells) showing GFP-Bgs4 intensity in vesicles from WT (blue) and *smi1-1* cells (red). Data in the right graph are mean ± SEM.

Several proteins have been identified as regulators of glucan synthases or glucanases (see *Introduction*). However, few proteins are known to regulate the localization of both classes of enzymes. Recently, Cdc42 GTPase was shown to promote recruitment of Bgs1 to the division site and be critical for proper localization of Eng1 and Agn1 (Onwubiko *et al.*, 2020). Here we showed that Smi1 is important for division-site localization of both glucan synthases and glucanases, suggesting an interesting dual role of Smi1 in septum integrity.

Most of our results indicate that Smi1 mainly regulates Bgs4 and the *smi1-1* phenotype more closely resembles that of Bgs4 than that of Bgs1 mutants. After culture at restrictive temperature, Bgs1 mutants display very slow or complete failure in actomyosin ring constriction (Liu *et al.*, 1999; Dundon and Pollard, 2020), as well as multiseptation and ring sliding due to less efficient anchoring (Arasada and Pollard, 2014; Cortes *et al.*, 2015). None of these characteristics was observed in the *smi1-1* mutant, and ring kinetics was not affected in *smi1-1* (Supplemental Figure S3). In contrast, the lysis

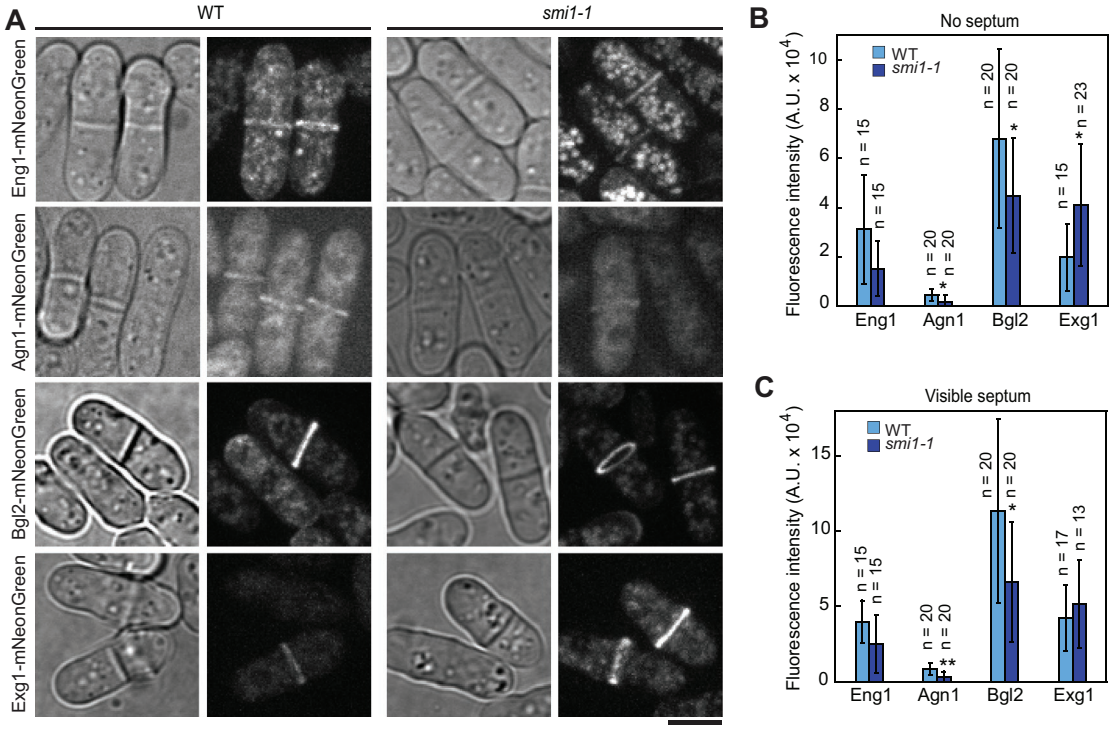

FIGURE 8: Localization and intensity of glucanases Eng1, Agn1, Bgl2, and Exg1 in *smi1-1* cells. (A–C) DIC and fluorescence confocal images (A) and quantifications of fluorescence intensity of Eng1, Agn1, Bgl2, and Exg1 in cells without (B) or with (C) visible septum under DIC. WT and *smi1-1* cells were grown for 2 h at 36°C. Scale bar, 5 µm. *$p < 0.01$, **$p < 0.001$ compared with the WT.

phenotype of *smi1-1* is very similar to that of Bgs4 mutants. Bgs4 is required for the proper synthesis of the cell wall surrounding the primary septum and compensates for excessive cell wall degradation during cell separation (Cortes *et al.*, 2005; Muñoz *et al.*, 2013). Bgs4 depletion leads to the absence of the lateral cell wall at the start of cell separation (Cortés *et al.*, 2016) and results in excessive cell wall degradation (Cortes *et al.*, 2005; Muñoz *et al.*, 2013), which was observed in *smi1-1* cells under electron microscopy (Figure 3). Despite all these similarities, cells lacking Bgs4 show phenotypic changes not seen in *smi1-1*, such as ring sliding, obliquely positioned rings and septa, and misdirected septum synthesis. Moreover, Bgs4 is essential for secondary septum formation and for correct primary septum completion (Muñoz *et al.*, 2013), which is not consistent with the *smi1* mutant phenotype. It is possible that the remaining Bgs4 at the division site in *smi1-1* is sufficient to maintain some of the Bgs4 functions.

We and others recently characterized Sbg1 as a regulator of glucan synthase Bgs1 (Davidson *et al.*, 2016; Sethi *et al.*, 2016). However, Smi1 differs from Sbg1 in how it regulates glucan synthases. First, Smi1 is an IDP (Figure 1, A and B), while Sbg1 is a transmembrane protein (Davidson *et al.*, 2016), which allows Sbg1 to localize as a stable ring at the division site during septum formation until abscission (Davidson *et al.*, 2016) and to link the plasma membrane, the actomyosin ring, and the division septum assembly machinery (Sethi *et al.*, 2016). In contrast, Smi1 accumulates transiently at the division site and localizes mostly in cytoplasmic vesicles (Figure 4, A–C) and is not involved in ring stability or kinetics (Supplemental Figure S3). Second, Sbg1 and Smi1 have different specificities. Sbg1 plays a specific role in Bgs1 localization and does not affect other glucan synthases (Davidson *et al.*, 2016), while Smi1 mainly regulates Bgs4 but also affects the localization of Bgs1 and Sbg1, as well as glucanases Agn1, Bgl2, and Exg1, thus playing a broader role in septum synthesis (Figures 7 and 8). The mechanism used by Smi1 to traffic Bgs4 to the division site still needs to be determined in future studies.

Smi1 proteins have diverse functions beyond cytokinesis

Our findings that Smi1 regulates septum integrity and the localization of Bgs4 and other proteins highlight some novel roles for Smi1. It has not previously been reported that Smi1 regulates glucan synthases or glucanases in budding yeast and other fungi. In *S. cerevisiae*, Smi1 acts as a hub that physically interacts with the key components of two pathways: Rho GTPase-protein kinase C-MAP kinase in the cell wall integrity pathway and the calcineurin phosphatase in the calcium–calcineurin pathway (Dagkessamanskaia *et al.*, 2010a,b; Martin-Yken *et al.*, 2016). It will be interesting to investigate in the future whether Smi1 regulates septum integrity through these pathways. Smi1 also regulates transcription of genes involved in cell cycle, cell wall synthesis, morphogenesis, and heat and cell wall stress in a variety of fungi (Martin-Yken *et al.*, 2002; Lagorce *et al.*, 2003; Penacho *et al.*, 2012). It will be interesting to determine whether Smi1 has these functions in fission yeast besides its role in cytokinesis, especially whether Smi1 also regulates Bgs4 transcription.

Smi1 has homologues throughout the fungal kingdom, but not in higher eukaryotes including humans, making the essential Smi1/Knr4 family proteins attractive targets for new antifungal drugs. In the human pathogen *Candida albicans,* Smi1 expression is induced in the pathogenic hyphal cells (Harcus *et al.*, 2004), and the *smi1*Δ/*smi1*Δ mutant shows reduced cell wall β-glucan synthesis and biofilm formation and less biofilm-associated fluconazole resistance (Nett *et al.*, 2011). Moreover, the functional interaction between *S. cerevisiae* Smi1 and calcineurin supports the potential importance of studying Smi1 as an antifungal target, because calcineurin

is implicated in the morphogenic switches responsible for virulence in pathogenic fungi (Martin-Yken *et al.*, 2003).

In conclusion, we found that Smi1 has at least two novel roles in cytokinesis: involvement in the cell wall integrity pathway and in recruiting glucan synthases and glucanases to the division site for successful septation. It will be interesting to determine whether these roles are also conserved in other fungi.

MATERIALS AND METHODS

Strain construction and genetic methods

All strains used in this study are listed in Supplemental Table S1. To delete or tag genes at their endogenous locations, we used PCR-based gene targeting by homologous recombination (Bähler *et al.*, 1998). All tagged proteins were expressed under their native promotors, except where specified. To deplete Smi1, we used the *P81nmt1* promoter, which is repressed by thiamine (Maundrell, 1990; Basi *et al.*, 1993). All *smi1* strains were tagged at their C-terminus, and their functionalities were confirmed by growing cells on YE5S and YE5S + phloxin B (PB) plates at 25°, 30°, and 36°C.

The temperature-sensitive *smi1-1* mutant was created using marker reconstitution mutagenesis (Tang *et al.*, 2011; Lee *et al.*, 2014). Briefly, *smi1* was cloned into a pHis5C plasmid, and this construct was used as a template in an error-prone PCR using a mutagenic cocktail (8 mM dTTP, 8 mM dCTP, 48 mM $MgCl_2$, and 5 mM $MnCl_2$). The PCR product was then transformed into strain JW9102 (*smi1-3'UTR-his5ΔC-kanMX6 his5Δ ade6-210 leu1-32 ura4*), and positive transformants were selected for histidine prototroph and temperature sensitivity at 36°C. Finally, we sequenced the mutants to identify the mutations in the *smi1* open reading frame (ORF). *smi1-1* showed three mutations: D307G, E331G, and N426S.

To mistarget Smi1, Bgs1, Bgs4, Ags1, or Sbg1 to mitochondria, strains expressing mEGFP/GFP-tagged proteins were crossed to a strain expressing the mitochondrial outer membrane protein Tom20 tagged with GBP (Yamamoto *et al.*, 2011).

Affinity purification and mass spectrometry

We purified the GFP fusion protein from *S. pombe* extracts to identify the Bgs4 binding partners. We expressed the GFP control under the *41nmt1* promoter and GFP-Bgs4 and GFP-Bgs1 under their native promoters. Cells were grown in YE5S medium at 25°C for 48 h. Lyophilized cells stored at –80°C were thawed and ground with pestle and mortar to a homogeneous fine powder at room temperature and mixed with cold immunoprecipitation buffer (50 mM HEPES, pH 7.5, 1% NP-40, 200 mM NaCl, 1 mM EDTA, 20 mM β-glycerophosphate, 0.1 mM Na_3VO_4, 50 mM NaF, 1 mM phenylmethylsulfonyl fluoride [PMSF], and one protease inhibitor tablet/50 ml buffer [Roche, Mannheim, Germany]). Cell extract was then centrifuged twice at 4°C (21,000 rpm for 30 min and 21,000 rpm for 10 min), and the protein concentration was measured via Bradford assay (Bio-Rad Laboratories, Hercules, CA). Then, cell extract was diluted with dilution/wash buffer (10 mM Tris-HCl, pH 7.5, 150 mM NaCl, 0.5 mM EDTA) and incubated with prewashed GFP-Trap magnetic agarose beads (Chromotek, Planegg-Martinsried, Germany) at 4°C for 2 h. Beads were washed five times with dilution/wash buffer and eluted with SDS-sample buffer (Laemmli) by boiling the beads for 5 min at 95°C. For mass spectrometry analysis, protein samples were run through a stacking SDS–PAGE gel (Liu *et al.*, 2010) and excised as a one-sample band, which was sent for mass spectrometry analysis at the Mass Spectrometry and Proteomics Facility at The Ohio State University, Columbus, OH.

For mass spectrometry, gel pieces were digested overnight at room temperature with 10 µg/ml trypsin (Promega, Madison, WI) in 50 mM ammonium bicarbonate. The peptides were extracted with 50% acetonitrile/5% formic acid. Peptides were dried in a vacufuge and resuspended in 20 µl of 50 mM acetic acid. Capillary-liquid chromatography-nanospray tandem mass spectrometry (capillary-LC/MS/MS) was performed on a Thermo Scientific Orbitrap Fusion equipped with an EASY-Spray Source operated in positive ion mode. Samples were separated on an easy spray nano column (Pepmap RSLC; C18, 3 µ, 100 A, 75 µm × 150 mm; Thermo Scientific) using a two-dimensional RSLC high-performance liquid chromatography system from Thermo Scientific. Mass spectrometry data were analyzed using Mascot Daemon by Matrix Science version 2.5.1 (Boston, MA) and searched against the most recent SwissProt or NCBI databases. The mass accuracy of the precursor ions was set to 10 ppm, and fragment mass tolerance was set to 0.5 Da. Considered variable modifications were oxidation (Met), deamidation (N and Q), and carbamidomethylation (Cys). Four missed cleavages for the enzyme were permitted. A decoy database was used to determine the false discovery rate (FDR), and peptides were filtered at FDR of 1%. Proteins identified with at least two unique peptides were considered for a reliable identification.

Cellular methods and pharmacological treatments

To stain the primary septum, we incubated cells with 10 µg/ml Calcofluor for 10 min in the dark before imaging. To compare the sensitivities of the WT and *smi1-1* cells to various stresses, cells were grown exponentially in YE5S medium at 25°C, serially (5×) diluted, and spotted onto YE5S plates and YE5S plates containing 100 µg/ml Calcofluor white, 0.0075% SDS, or 0.0075% SDS + 1 M sorbitol, and incubated at 36°C for 48 h.

Microscopy and image analyses

Strains stored at –80°C were streaked onto YE5S plates and grown for 2 days at 25°C. Fresh cells were inoculated into YE5S liquid media and grown exponentially for ~2 days at 25°C. When indicated, cells were transferred to YE5S + thiamine medium to repress the *nmt1* promoters. For microscopy, cells were collected by centrifugation at 3000 rpm for 30 s, washed once with EMM5S to reduce autofluorescence and once with EMM5S plus 5 µM *n*-propyl-gallate (to reduce phototoxicity and photobleaching during imaging). Cells were then imaged on a thin EMM5S with 20% gelatin pad with 5 µM *n*-propyl-gallate. For imaging at 36°C, the cells were cultivated in liquid culture at 25°C and then shifted to 36°C for the indicated time. Cells were then collected (3000 rpm, 30 s), placed on a prewarmed coverglass-bottom dish (0420041500C; Bioptechs, Butler, PA), and covered with prewarmed YE5S agar before being imaged at 36°C in a temperature-controlled chamber (Stage Top Incubator INUB-PPZI2-F1 with UNIV2-D35 dish holder; Tokai Hit, Shizuoka-ken, Japan).

For fluorescence images and time-lapse movies, microscopy was performed as previously described. Briefly, we used a spinning-disk confocal system (UltraVIEW Vox CSUX1 system; PerkinElmer, Waltham, MA) with 440-, 488-, 515-, and 561-nm solid-state lasers and back thinned electron-multiplying charge-coupled device (EMCCD) cameras (C9100-13 or C9100-23B; Hamamatsu Photonics, Bridgewater, NJ) on a Nikon Ti-E microscope. Nikon Plan-Apo oil objective lenses of 100×/1.4 or 100×/1.45 numerical aperture (NA) were used. When only differential interference contrast (DIC) images were taken, we used a Nikon Eclipse Ti inverted microscopy equipped with a DS-QI1 Nikon cooled digital camera (Nikon, Melville, NY).

TIRF microscopy was used to track the movement of GFP-Bgs4 and Smi1-tdTomato cytoplasmic puncta simultaneously. Images were collected using a Nikon Eclipse Ti-E microscope equipped with a Nikon TIRF illuminator, Nikon perfect focus system, a Nikon Plan Apo 100×/1.45 NA oil objective, and an iXon Ultra 897 EMCCD camera (Andor Technology) controlled with NIS Elements software (Nikon, Melville, NY).

Microscopy images were analyzed using Volocity (PerkinElmer) and ImageJ (National Institutes of Health, Bethesda, MD) (Schneider *et al.*, 2012). Fluorescence images shown in the figures are maximum-intensity projections of image stacks with 0.4–0.6 µm spacing except where indicated. For intensity quantification, only cells within the central ~75% of the imaging field were used to reduce interference from uneven illumination. To measure the global protein level in a whole cell using the fluorescence intensity, the polygon region of interest (ROI) tool in ImageJ was applied to trace cell boundaries. Then, the fluorescence intensity in WT cells with no fluorescent tag was used to deduct the background. For quantification of fluorescence intensity at the division site, a rectangular ROI1 (~4 μm^2) was drawn at the division site to measure the mean intensity. Another rectangular ROI2 approximately twice the size of ROI1 elongated along the cell long axis was drawn to calculate cytoplasmic background as described (Wu and Pollard, 2005; Zhu *et al.*, 2013; Coffman and Wu, 2014). Tracking of vesicles moving toward the division site was performed manually using ImageJ. For vesicle colocalization analysis, the plot profile in both channels was analyzed using ImageJ, and the distance between the peak of profiles, which was considered the centroid of a vesicle, was calculated. If the distance was less than the vesicle radius, we considered the vesicles as colocalized. Data in the figures represent mean values ± SD unless otherwise described. Graphs were made in KaleidaGraph software, and the *p* values were calculated using a two-tailed Student's *t* test.

Electron microscopy

We used electron microscopy to investigate cell wall and septum morphology in WT (JW81), *smi1-1*, and *81nmt1-smi1* strains. Cells were grown in YE5S + thiamine medium exponentially for 48 h at 25˚C and then fixed with 2.5% glutaraldehyde in phosphate buffer (0.1 M sodium phosphate, pH 7.4, and 0.1 M sucrose) for 1 h. The fixed cells were submitted to the Campus Microscopy and Imaging Facility at The Ohio State University, where the samples were further fixed with 1% osmium tetroxide, embedded in agarose block, dehydrated in alcohol, and embedded in Epon8 epoxy resin as described before (Hayat, 1986). Thin sections of 70–90 nm were cut with a Leica EM UC6 ultramicrotome. Sections were stained with uranyl acetate and lead citrate and imaged using a FEI Tecnai G2 Spirit transmission electron microscope at 80 kV (Watanabe *et al.*, 1988; Hayat, 2000).

Coimmunoprecipitation and Western blotting

We carried out coimmunoprecipitation and Western blotting similarly to previously described methods (Cortes *et al.*, 2012; Lee and Wu, 2012; Gerien *et al.*, 2020). Lyophilized cells (200 mg) of each strain were ground into fine powder. For whole cell protein extracts, cell powder was dissolved with lysis buffer (50 mM Tris-HCl, pH 7.5, 5 mM EDTA, 200 mM NaCl, 0.5% Tween 20, 100 µM PMSF, and protease inhibitor [1 tablet/50 ml; Roche]), and proteins were separated by SDS–PAGE before Western blotting. For protein extracts from membrane enriched fractions, cell powder was dissolved with 2 ml lysis buffer without detergent (50 mM Tris-HCl, pH 7.5, 5 mM EDTA, 200 mM NaCl, 100 µM PMSF, and cocktail protease inhibitor). Then the cell lysates were centrifuged for two rounds at 4500 × *g* for 1 min and 16,000 × *g* for 1 h at 4°C, respectively. The pellet containing the membrane fraction from the second centrifugation was resuspended in 600 µl of immunoprecipitation buffer (50 mM Tris-HCl, pH 7.5, 5 mM EDTA, 200 mM NaCl, 0.5% Tween 20, 100 µM PMSF, and cocktail protease inhibitor). Next, the membrane suspension was centrifuged (21,000 × *g*, 30 min, 4°C) and the supernatant was collected. The solubilized membrane proteins were incubated with 30 µl of protein G magnetic beads (Invitrogen) bound with polyclonal anti-GFP antibody (Novus Biologicals) at 4°C for 2 h. The beads were washed with 1 ml immunoprecipitation buffer three times and then resuspended in sample buffer.

Proteins were separated by 4–20% Tris-glycine gradient SDS–PAGE (Mini-PROTEAN; Bio-Rad) and transferred to Immobilon-P membrane (Millipore). The membrane was blotted to detect GFP- or 13Myc-tagged proteins with the corresponding antibodies (monoclonal anti-GFP; 1:1000; [Roche]; and monoclonal anti-Myc; 1:2000; [Roche]) and the enhanced chemiluminescence (ECL) detection kit (SuperSignal; Thermo Scientific). α-TAT1 (1:20,000 dilution) was used as a loading control (Woods *et al.*, 1989).

ACKNOWLEDGMENTS

We thank Mohan Balasubramanian, Kathy Gould, Sophie Martin, Thomas Pollard, and Takashi Toda for strains; the Stephen Osmani and Dmitri Kudryashov laboratories for equipment; the Campus Microscopy and Imaging Facility, Mass Spectrometry and Proteomics Facility, and Samantha Nusbaum and Tiffany Ko at The Ohio State University for technical support; and current and past members of the Wu laboratory for helpful discussions and suggestions. The Fusion Orbitrap instrument was supported by National Institutes of Health (NIH) grant S10 OD018056. The work was supported by the National Institute of General Medical Sciences of the NIH (grant R01 GM118746 to J.-Q.W.) and Pelotonia (Postdoctoral fellowships to L.V.G.L and S. Z and an Undergraduate fellowship to E.G.G). The content is solely the responsibility of the authors and does not necessarily represent the official views of the National Institutes of Health or Pelotonia.

REFERENCES

Alonso-Nunez ML, An H, Martin-Cuadrado AB, Mehta S, Petit C, Sipiczki M, del Rey F, Gould KL, de Aldana CR (2005). Ace2p controls the expression of genes required for cell separation in *Schizosaccharomyces pombe*. Mol Biol Cell 16, 2003–2017.

Arasada R, Pollard TD (2014). Contractile ring stability in *S. pombe* depends on F-BAR protein Cdc15p and Bgs1p transport from the Golgi complex. Cell Rep 8, 1533–1544.

Arasada R, Pollard TD (2015). A role for F-BAR protein Rga7p during cytokinesis in *S. pombe*. J Cell Sci 128, 2259–2268.

Arellano M, Duran A, Perez P (1996). Rho1 GTPase activates the (1-3)β-D-glucan synthase and is involved in *Schizosaccharomyces pombe* morphogenesis. EMBO J 15, 4584–4591.

Bähler J, Wu J-Q, Longtine MS, Shah NG, McKenzie A III, Steever AB, Wach A, Philippsen P, Pringle JR (1998). Heterologous modules for efficient and versatile PCR-based gene targeting in *Schizosaccharomyces pombe*. Yeast 14, 943–951.

Balasubramanian MK, McCollum D, Chang L, Wong KC, Naqvi NI, He X, Sazer S, Gould KL (1998). Isolation and characterization of new fission yeast cytokinesis mutants. Genetics 149, 1265–1275.

Basi G, Schmid E, Maundrell K (1993). TATA box mutations in the *Schizosaccharomyces pombe nmt1* promoter affect transcription efficiency but not the transcription start point or thiamine repressibility. Gene 123, 131–136.

Beauvais A, Bruneau JM, Mol PC, Buitrago MJ, Legrand R, Latge JP (2001). Glucan synthase complex of *Aspergillus fumigatus*. J Bacteriol 183, 2273–2279.

Calonge TM, Nakano K, Arellano M, Arai R, Katayama S, Toda T, Mabuchi I, Perez P (2000). *Schizosaccharomyces pombe* Rho2p GTPase regulates

cell wall α-glucan biosynthesis through the protein kinase Pck2p. Mol Biol Cell 11, 4393–4401.
Cheng H, Sugiura R, Wu W, Fujita M, Lu Y, Sio SO, Kawai R, Takegawa K, Shuntoh H, Kuno T (2002). Role of the Rab GTP-binding protein Ypt3 in the fission yeast exocytic pathway and its connection to calcineurin function. Mol Biol Cell 13, 2963–2976.
Coffman VC, Wu J-Q (2014). Every laboratory with a fluorescence microscope should consider counting molecules. Mol Biol Cell 25, 1545–1548.
Cortes JC, Carnero E, Ishiguro J, Sanchez Y, Duran A, Ribas JC (2005). The novel fission yeast (1,3)β-D-glucan synthase catalytic subunit Bgs4p is essential during both cytokinesis and polarized growth. J Cell Sci 118, 157–174.
Cortes JC, Ishiguro J, Duran A, Ribas JC (2002). Localization of the (1,3)β-D-glucan synthase catalytic subunit homologue Bgs1p/Cps1p from fission yeast suggests that it is involved in septation, polarized growth, mating, spore wall formation and spore germination. J Cell Sci 115, 4081–4096.
Cortes JC, Pujol N, Sato M, Pinar M, Ramos M, Moreno B, Osumi M, Ribas JC, Perez P (2015). Cooperation between paxillin-like protein Pxl1 and glucan synthase Bgs1 is essential for actomyosin ring stability and septum formation in fission yeast. PLoS Genet 11, e1005358.
Cortes JC, Sato M, Munoz J, Moreno MB, Clemente-Ramos JA, Ramos M, Okada H, Osumi M, Duran A, Ribas JC (2012). Fission yeast Ags1 confers the essential septum strength needed for safe gradual cell abscission. J Cell Biol 198, 637–656.
Cortés JCG, Ramos M, Osumi M, Pérez P, Ribas JC (2016). Fission yeast septation. Commun Integr Biol 9, e1189045.
Costanzo M, Baryshnikova A, Bellay J, Kim Y, Spear ED, Sevier CS, Ding H, Koh JL, Toufighi K, Mostafavi S, *et al*. (2010). The genetic landscape of a cell. Science 327, 425–431.
Dagkessamanskaia A, Durand F, Uversky VN, Binda M, Lopez F, El Azzouzi K, Francois JM, Martin-Yken H (2010a). Functional dissection of an intrinsically disordered protein: understanding the roles of different domains of Knr4 protein in protein-protein interactions. Protein Sci 19, 1376–1385.
Dagkessamanskaia A, El Azzouzi K, Kikuchi Y, Timmers T, Ohya Y, Francois JM, Martin-Yken H (2010b). Knr4 N-terminal domain controls its localization and function during sexual differentiation and vegetative growth. Yeast 27, 563–574.
Davidson R, Laporte D, Wu J-Q (2015). Regulation of Rho-GEF Rgf3 by the arrestin Art1 in fission yeast cytokinesis. Mol Biol Cell 26, 453–466.
Davidson R, Pontasch JA, Wu J-Q (2016). Sbg1 is a novel regulator for the localization of the β-glucan synthase Bgs1 in fission yeast. PLoS One 11, e0167043.
Dekker N, Speijer D, Grun CH, van den Berg M, de Haan A, Hochstenbach F (2004). Role of the α-glucanase Agn1p in fission-yeast cell separation. Mol Biol Cell 15, 3903–3914.
de Leon N, Sharifmoghadam MR, Hoya M, Curto MA, Doncel C, Valdivieso MH (2013). Regulation of cell wall synthesis by the clathrin light chain is essential for viability in *Schizosaccharomyces pombe*. PLoS One 8, e71510.
Drgonova J, Drgon T, Tanaka K, Kollar R, Chen GC, Ford RA, Chan CS, Takai Y, Cabib E (1996). Rho1p, a yeast protein at the interface between cell polarization and morphogenesis. Science 272, 277–279.
Duenas-Santero E, Martin-Cuadrado AB, Fontaine T, Latge JP, del Rey F, Vazquez de Aldana C (2010). Characterization of glycoside hydrolase family 5 proteins in *Schizosaccharomyces pombe*. Eukaryot Cell 9, 1650–1660.
Dundon SER, Pollard TD (2020). Microtubule nucleation promoters Mto1 and Mto2 regulate cytokinesis in fission yeast. Mol Biol Cell 31, 1846–1856.
Gerien KS, Zhang S, Russell AC, Zhu Y-H, Purde V, Wu J-Q (2020). Roles of Mso1 and the SM protein Sec1 in efficient vesicle fusion during fission yeast cytokinesis. Mol Biol Cell 31, 1570–1583.
Goehring AS, Mitchell DA, Tong AH, Keniry ME, Boone C, Sprague GF Jr (2003). Synthetic lethal analysis implicates Ste20p, a p21-activated potein kinase, in polarisome activation. Mol Biol Cell 14, 1501–1516.
Harcus D, Nantel A, Marcil A, Rigby T, Whiteway M (2004). Transcription profiling of cyclic AMP signaling in *Candida albicans*. Mol Biol Cell 15, 4490–4499.
Harrison JC, Bardes ES, Ohya Y, Lew DJ (2001). A role for the Pkc1p/Mpk1p kinase cascade in the morphogenesis checkpoint. Nat Cell Biol 3, 417–420.
Hayat M (1986). Basic Techniques for Transmission Electron Microscopy, San Diego, CA: Academic Press.
Hayat MA (2000). Principles and Techniques of Electron Microscopy: Biological Applications, Cambridge, UK: Cambridge University Press, p. 543.
Hayles J, Wood V, Jeffery L, Hoe KL, Kim DU, Park HO, Salas-Pino S, Heichinger C, Nurse P (2013). A genome-wide resource of cell cycle and cell shape genes of fission yeast. Open Biol 3, 130053.
Katayama S, Hirata D, Arellano M, Perez P, Toda T (1999). Fission yeast α-glucan synthase Mok1 requires the actin cytoskeleton to localize the sites of growth and plays an essential role in cell morphogenesis downstream of protein kinase C function. J Cell Biol 144, 1173–1186.
Kim DU, Hayles J, Kim D, Wood V, Park HO, Won M, Yoo HS, Duhig T, Nam M, Palmer G, *et al*. (2010). Analysis of a genome-wide set of gene deletions in the fission yeast *Schizosaccharomyces pombe*. Nat Biotech 28, 617–623.
Kondoh O, Tachibana Y, Ohya Y, Arisawa M, Watanabe T (1997). Cloning of the *RHO1* gene from *Candida albicans* and its regulation of β-1,3-glucan synthesis. J Bacteriol 179, 7734–7741.
Lagorce A, Hauser NC, Labourdette D, Rodriguez C, Martin-Yken H, Arroyo J, Hoheisel JD, Francois J (2003). Genome-wide analysis of the response to cell wall mutations in the yeast *Saccharomyces cerevisiae*. J Biol Chem 278, 20345–20357.
Lee DW, Ahn GW, Kang HG, Park HM (1999). Identification of a gene, *SOO1*, which complements osmo-sensitivity and defect in *in vitro* β-1,3-glucan synthase activity in *Saccharomyces cerevisiae*. Biochim Biophys Acta 1450, 145–154.
Lee H-H, Park J-S, Chae SK, Maeng PJ, Park HM (2002). *Aspergillus nidulans* sod^{VI}*C1* mutation causes defects in cell wall biogenesis and protein secretion. FEMS Microbiol Lett 208, 253–257.
Lee I-J, Wang N, Hu W, Schott K, Bähler J, Giddings TH, Pringle JR, Du L-L, Wu J-Q (2014). Regulation of spindle pole body assembly and cytokinesis by the centrin-binding protein Sfi1 in fission yeast. Mol Biol Cell 25, 2735–2749.
Lee I-J, Wu J-Q (2012). Characterization of Mid1 domains for targeting and scaffolding in fission yeast cytokinesis. J Cell Sci 125, 2973–2985.
Liu H-L, Osmani AH, Ukil L, Son S, Markossian S, Shen KF, Govindaraghavan M, Varadaraj A, Hashmi SB, De Souza CP, *et al*. (2010). Single-step affinity purification for fungal proteomics. Eukaryot Cell 9, 831–833.
Liu J, Wang H, McCollum D, Balasubramanian MK (1999). Drc1p/Cps1p, a 1,3-β-glucan synthase subunit, is essential for division septum assembly in *Schizosaccharomyces pombe*. Genetics 153, 1193–1203.
Liu Y, Lee I-J, Sun M, Lower CA, Runge KW, Ma J, Wu J-Q (2016). Roles of the novel coiled-coil protein Rng10 in septum formation during fission yeast cytokinesis. Mol Biol Cell 27, 2528–2541.
Liu Y, McDonald NA, Naegele SM, Gould KL, Wu J-Q (2019). The F-BAR domain of Rga7 relies on a cooperative mechanism of membrane binding with a partner protein during fission yeast cytokinesis. Cell Rep 26, 2540–2548.
Martin-Cuadrado AB, Duenas E, Sipiczki M, Vazquez de Aldana CR, del Rey F (2003). The endo-β-1,3-glucanase Eng1p is required for dissolution of the primary septum during cell separation in *Schizosaccharomyces pombe*. J Cell Sci 116, 1689–1698.
Martin-Yken H, Dagkessamanskaia A, Basmaji F, Lagorce A, Francois J (2003). The interaction of Slt2 MAP kinase with Knr4 is necessary for signalling through the cell wall integrity pathway in *Saccharomyces cerevisiae*. Mol Microbiol 49, 23–35.
Martin-Yken H, Dagkessamanskaia A, Talibi D, Francois J (2002). KNR4 is a member of the PKC1 signalling pathway and genetically interacts with *BCK2*, a gene involved in cell cycle progression in *Saccharomyces cerevisiae*. Curr Genet 41, 323–332.
Martin-Yken H, Francois JM, Zerbib D (2016). Knr4: a disordered hub protein at the heart of fungal cell wall signalling. Cell Microbiol 18, 1217–1227.
Maundrell K (1990). *nmt1* of fission yeast. A highly transcribed gene completely repressed by thiamine. J Biol Chem 265, 10857–10864.
Meitinger F, Palani S (2016). Actomyosin ring driven cytokinesis in budding yeast. Semin Cell Dev Biol 53, 19–27.
Miyakawa T, Mizunuma M (2007). Physiological roles of calcineurin in *Saccharomyces cerevisiae* with special emphasis on its roles in G2/M cell-cycle regulation. Biosci Biotechnol Biochem 71, 633–645.
Mizunuma M, Hirata D, Miyaoka R, Miyakawa T (2001). GSK-3 kinase Mck1 and calcineurin coordinately mediate Hsl1 down-regulation by Ca^{2+} in budding yeast. EMBO J 20, 1074–1085.
Motegi F, Arai R, Mabuchi I (2001). Identification of two type V myosins in fission yeast, one of which functions in polarized cell growth and moves rapidly in the cell. Mol Biol Cell 12, 1367–1380.
Muñoz J, Cortés JCG, Sipiczki M, Ramos M, Clemente-Ramos JA, Moreno MB, Martins IM, Pérez P, Ribas JC (2013). Extracellular cell wall β(1,3)-glucan is required to couple septation to actomyosin ring contraction. J Cell Biol 203, 265–282.

Nakano K, Mutoh T, Mabuchi I (2001). Characterization of GTPase-activating proteins for the function of the Rho-family small GTPases in the fission yeast *Schizosaccharomyces pombe*. Genes Cells 6, 1031–1042.
Nett JE, Sanchez H, Cain MT, Ross KM, Andes DR (2011). Interface of *Candida albicans* biofilm matrix-associated drug resistance and cell wall integrity regulation. Eukaryot Cell 10, 1660–1669.
Onwubiko UN, Rich-Robinson J, Mustaf RA, Das ME (2020). Cdc42 promotes Bgs1 recruitment for septum synthesis and glucanase localization for cell separation during cytokinesis in fission yeast. Small GTPases 12, 257–264.
Penacho V, Blondin B, Valero E, Gonzalez R (2012). Flocculation and transcriptional adaptation to fermentation conditions in a recombinant wine yeast strain defective for *KNR4/SMI1*. Biotechnol Prog 28, 327–336.
Pollard TD (2019). Cell motility and cytokinesis: from mysteries to molecular mechanisms in five decades. Annu Rev Cell Dev Biol 35, 1–28.
Proctor SA, Minc N, Boudaoud A, Chang F (2012). Contributions of turgor pressure, the contractile ring, and septum assembly to forces in cytokinesis in fission yeast. Curr Biol 22, 1601–1608.
Ribas JC, Diaz M, Duran A, Perez P (1991). Isolation and characterization of *Schizosaccharomyces pombe* mutants defective in cell wall (1-3)β-D-glucan. J Bacteriol 173, 3456–3462.
Rothbauer U, Zolghadr K, Muyldermans S, Schepers A, Cardoso MC, Leonhardt H (2008). A versatile nanotrap for biochemical and functional studies with fluorescent fusion proteins. Mol Cell Proteomics 7, 282–289.
Sajiki K, Hatanaka M, Nakamura T, Takeda K, Shimanuki M, Yoshida T, Hanyu Y, Hayashi T, Nakaseko Y, Yanagida M (2009). Genetic control of cellular quiescence in *S. pombe*. J Cell Sci 122, 1418–1429.
Salimova E, Sohrmann M, Fournier N, Simanis V (2000). The *S. pombe* orthologue of the *S. cerevisiae mob1* gene is essential and functions in signalling the onset of septum formation. J Cell Sci 113, 1695–1704.
Schneider CA, Rasband WS, Eliceiri KW (2012). NIH Image to ImageJ: 25 years of image analysis. Nat Methods 9, 671–675.
Sethi K, Palani S, Cortes JC, Sato M, Sevugan M, Ramos M, Vijaykumar S, Osumi M, Naqvi NI, Ribas JC, *et al.* (2016). A new membrane protein Sbg1 links the contractile ring apparatus and septum synthesis machinery in fission yeast. PLoS Genet 12, e1006383.
Tang X, Huang J, Padmanabhan A, Bakka K, Bao Y, Tan BY, Cande WZ, Balasubramanian MK (2011). Marker reconstitution mutagenesis: a simple and efficient reverse genetic approach. Yeast 28, 205–212.
Thiyagarajan S, Munteanu EL, Arasada R, Pollard TD, O'Shaughnessy B (2015). The fission yeast cytokinetic contractile ring regulates septum shape and closure. J Cell Sci 128, 3672–3681.
Toda T, Shimanuki M, Yanagida M (1993). Two novel protein kinase C-related genes of fission yeast are essential for cell viability and implicated in cell shape control. EMBO J 12, 1987–1995.
Viana RA, Pinar M, Soto T, Coll PM, Cansado J, Perez P (2013). Negative functional interaction between cell integrity MAPK pathway and Rho1 GTPase in fission yeast. Genetics 195, 421–432.
Vjestica A, Tang XZ, Oliferenko S (2008). The actomyosin ring recruits early secretory compartments to the division site in fission yeast. Mol Biol Cell 19, 1125–1138.
Watanabe S, Sasaki J, Wada T, Tanaka Y, Otsuka N (1988). Low gel temperature agarose encapsulation of small specimens for electron microscopy. J Electron Microsc (Tokyo) 37, 89–91.
Win TZ, Gachet Y, Mulvihill DP, May KM, Hyams JS (2001). Two type V myosins with non-overlapping functions in the fission yeast *Schizosaccharomyces pombe*: Myo52 is concerned with growth polarity and cytokinesis, Myo51 is a component of the cytokinetic actin ring. J Cell Sci 114, 69–79.
Woods A, Sherwin T, Sasse R, MacRae TH, Baines AJ, Gull K (1989). Definition of individual components within the cytoskeleton of *Trypanosoma brucei* by a library of monoclonal antibodies. J Cell Sci 93, 491–500.
Wu J-Q, Pollard TD (2005). Counting cytokinesis proteins globally and locally in fission yeast. Science 310, 310–314.
Yamamoto H, Itoh N, Kawano S, Yatsukawa Y, Momose T, Makio T, Matsunaga M, Yokota M, Esaki M, Shodai T, *et al*. (2011). Dual role of the receptor Tom20 in specificity and efficiency of protein import into mitochondria. Proc Natl Acad Sci USA 108, 91–96.
Zhou Z, Munteanu EL, He J, Ursell T, Bathe M, Huang KC, Chang F, Steinberg G (2015). The contractile ring coordinates curvature-dependent septum assembly during fission yeast cytokinesis. Mol Biol Cell 26, 78–90.
Zhu Y-H, Hyun J, Pan Y-Z, Hopper JE, Rizo J, Wu J-Q (2018). Roles of the fission yeast UNC-13/Munc13 protein Ync13 in late stages of cytokinesis. Mol Biol Cell 29, 2259–2279.
Zhu Y-H, Ye Y, Wu Z, Wu J-Q (2013). Cooperation between Rho-GEF Gef2 and its binding partner Nod1 in the regulation of fission yeast cytokinesis. Mol Biol Cell 24, 3187–3204.